Journal of Zhejiang University-SCIENCE A (Applied Physics & Engineering)
ISSN 1673-565X (Print); ISSN 1862-1775 (Online)
www.zju.edu.cn/jzus; www.springerlink.com
E-mail: jzus@zju.edu.cn

Method for determining effective flame emissivity in a rotary kiln incinerator burning solid waste*

Jin-cai DU[1,2], Qun-xing HUANG[†‡1], Jian-hua YAN[1]

([1]*State Key Laboratory of Clean Energy Utilization, Zhejiang University, Hangzhou 310027, China*)

([2]*School of Aeronautics and Astronautics, Zhejiang University, Hangzhou 310027, China*)

[†]E-mail: hqx@zju.edu.cn

Received July 4, 2012; Revision accepted Oct. 25, 2012; Crosschecked Nov. 16, 2012

Abstract: Temperature is the most important parameter for the improvement of combustion efficiency and the control of pollutants. In order to obtain accurate flame temperatures in a rotary kiln incinerator using non-intrusive thermographic method, the effective flame emissivity was studied. A combined narrow- and wide-band model and Mie scattering method were used to calculate the radiative properties for gases and fly-ash particles under different combustion conditions. The effects of the air/waste ratio and fly-ash particles on the effective flame emissivity were discussed. The results of numerical calculations showed that the effective emissivity decreased from 0.90 to 0.80 when the air/waste ratio increased from 1.0 to 1.8, and the effect of the fly-ash particles was ignorable under the conditions discussed in this paper. Experimental measurement results indicated that the accuracy of the thermographic temperature measurements improved significantly if the setting of the flame emissivity was adjusted according to the air/waste ratio.

Key words: Thermographic temperature measurement, Effective flame emissivity, Rotary kiln incinerator, Air/waste equivalence ratio

doi:10.1631/jzus.A1200168 **Document code:** A **CLC number:** TK124

1 Introduction

In the last decade, about 50 million kilograms of hazardous solid waste were generated in China each year (China Statistical Yearbook on Environment, 2009). According to the pollution control standard for hazardous waste incineration (GB 18484-2001) and the technical specifications for centralized incineration facility construction for hazardous waste (HJ/T176-2005), all hazardous solid waste must be burned in high-temperature incinerators using a rotary kiln as the primary combustion chamber. Because the waste components and heat values are changing all the time, the temperature of the incineration flame in the rotary kiln should be measured accurately and rapidly for stable operation and safety of the incinerator. More importantly, an accurate flame temperature is the most useful information for improving incineration efficiency and reducing pollutants (Buekens *et al.*, 1998). As a result of movement of the kiln and the harsh measurement conditions, industrial thermocouples installed at the front and rear ends of the kiln are widely used as the only temperature detectors (Docquier and Candel, 2002). The most notable disadvantages of a thermocouple are that, first, the flame temperature in the incinerator is non-uniform because of flame turbulence and the large geometric size of the kiln. The single-point temperature value obtained using a thermocouple is far from the overall actual flame temperature (Ballester *et al.*, 2010). Second, high-temperature solid particles in the flame

‡ Corresponding author

* Project supported by the National Basic Research Program (973) of China (Nos. 2009CB219802 and 2011CB201500), the National Water Pollution Control and Management Technology Major Projects (No. 2009ZX07317), and the Solid Waste Creative Team Project of Zhejiang Province (No. A2009R50049), China

will deposit on the thermocouple cover and gradually increase its response time, and will cause measurements to be unreliable. In the past few years, the poor performances of thermocouples have caused many waste incineration systems to suffer from slagging, refractory failure, and other incineration control problems (Manca and Rovaglio, 2002). Some systems cannot meet the pollution control standards for hazardous waste incineration and become another emission source of polychlorinated dibenzo-*p*-dioxin and polychlorinated dibenzofuran (Ni *et al.*, 2009). To obtain accurate flame temperatures in rotary kiln incinerators, many researchers have turned to non-intrusive thermographic temperature measurement techniques using infrared cameras, which are also capable of providing 2D flame temperature distributions. The thermographic method is fast and very attractive for temperature measurements under restricted measurement conditions. For example, a solid waste mass burning plant in Germany employed an infrared thermographic camera along with a fuzzy logic system to regulate the under-fire oxygen concentration, which was adjusted in each grate zone to respond to the inhomogeneity of the waste (Gohlke and Busch, 2001). A simultaneous inner and outer thermographic imaging system has been successfully used to control over-temperature slagging in an industrial waste incinerator to prolong the lifetime of refractory bricks (Vosteen *et al.*, 2002). Subramanya and Choudhuri (2004) proposed a dynamic zonal technique for evaluating the equivalence ratio from infrared flame imaging using a dynamic tracking method.

The main problem with thermographic temperature measurements is that the measurement accuracy depends significantly on the choice of flame emissivity in the infrared spectral range of the camera, and because of the poor understanding of the radiative properties of heterogeneous flames in the incinerator, most thermographic temperature measurements have treated the flame radiative emissivity as a constant value (Manca and Rovaglio, 2002; Ballester *et al.*, 2010). Although the radiative properties of pure gases and particles have been explored intensively for many years (Edwards, 1962; Edwards and Balakrishnan, 1973; Li and Tong, 1995; Modest, 2003), only a few reports have dealt with the emissivity of non-laboratory heterogeneous combustion flames, especially in the infrared range. Chang and Rhodes (1995) proposed a mathematical model for studying the effects of various particulates on flame radiative properties in solid waste incinerators. Planas-Cuchi *et al.* (2003) measured the emissivity of a liquid hydrocarbon pool flame using an infrared camera, and proposed a new correlation for the estimation of flame emissivities with different fire diameters. Sudheer and Prabhu (2010) investigated gasoline pool fires and found that the emissivity at the flame tip was lower than that at the base of the pool fire. Águeda *et al.* (2010) discussed the emissivity of a forest-wood-fueled fire, and according to their results, only flames thicker than 3.2 m exhibited an emissivity close to that of a blackbody (0.9), and the associated extinction coefficient was 0.72. Parent *et al.* (2010) investigated the emission of a vegetation flame and found that the radiative emission contribution from soot particles was relatively weak compared with those of the gas components in the infrared region. The above discussion provides useful information on the radiative emission characteristics of heterogeneous flames.

In this study, the effective emissivity of a heterogeneous flame in a commercial industrial waste incinerator using a rotary kiln was fully investigated under different burning conditions. A gas absorption band model and Mie method were used to determine the radiative properties of gases and fly-ash particles, respectively. The concentrations of gas and particles in the flame were obtained from mass and energy balance calculations by taking the waste burnout rate and air/waste equivalence ratio into consideration. The effects of particles and air/waste ratio on the effective flame emissivity were discussed.

2 Incineration facility and waste character

The incineration plant discussed in this study is located north of Hangzhou city and has been operating since 2008. The rotary kiln, also called the primary oxidation chamber, is a refractory-bricked, horizontal steel drum with an inside diameter of 3.0 m and a length of 9.0 m. Fig. 1a shows a photograph of the kiln. The kiln is rotated by a reversible driver of controllable speed. A diesel burner provides the energy to heat the interior of the kiln to the ignition

temperature of the waste at startup, and to maintain the temperature when the heat value of the waste is insufficient. The primary oxidation air is fed in through the burner and the secondary air can be supplied through a damper in the front of the kiln. The hazardous waste is fed in using a hydraulically driven piston and moves as a segment along the kiln. The slag is discharged at the end of the kiln into a conveyer under cooling water. The gases evolved in the kiln flow to the secondary oxidation chamber, where complete combustion occurs. A schematic diagram of the incineration system is shown in Fig. 1b. The stationary thermocouples A and B act as temperature detectors for combustion monitoring and incinerator control.

The throughput capacity of the incinerator, which depends on the combustible components in the waste, is approximately 2000 kg/h and the heat value of the waste reaches 13 000 kJ/kg. Table 1 shows an approximate analysis of a typical batch of waste and Table 2 gives the average ultimate analysis of the waste. In the following section, these data are used to calculate the concentrations of gases and fly-ash particles.

Since the incinerator was put into operation, several mal-operation accidents caused by incorrect flame temperatures from the thermocouples have occurred. In order to avoid further operational problems, an infrared camera was used, as shown in Fig. 1b. However, the measurement accuracy of a thermographic camera significantly depends on the choice of flame emissivity within the sensitive spectral range of the camera. The purpose of this study is to investigate the radiative properties of the flame and to determine the effective flame emissivity under different combustion conditions for accurate temperature measurement.

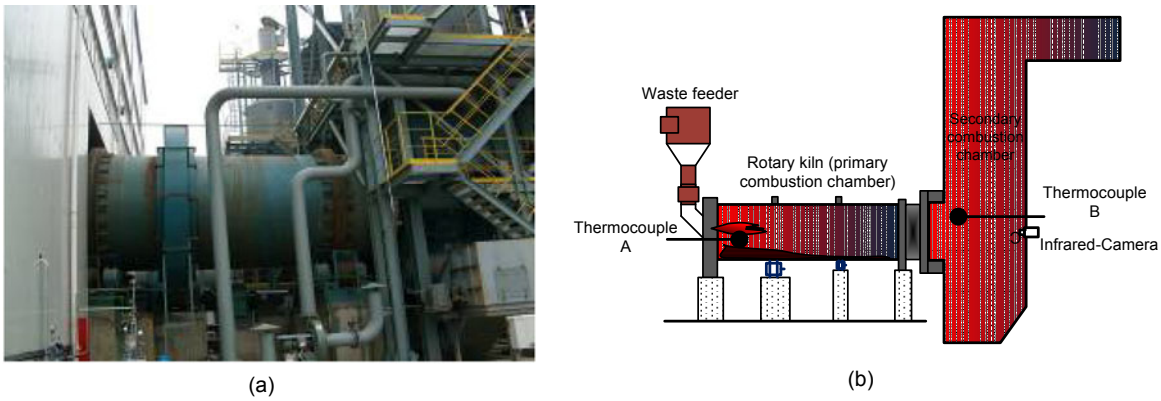

Fig. 1 Hazardous waste incineration system using a rotary kiln as primary combustion chamber
(a) Photograph of kiln incinerator; (b) Schematic diagram

Table 1 Approximate analyses of different hazardous wastes

Item	Moisture (%)	Ash (%)	Volatiles (%)	Fixed carbon (%)	Heat value (kJ/kg)
Tannery sludge	70.00	13.89	13.75	2.37	8062.54
Waste pesticide	5.00	7.74	66.40	20.85	13 328.69
Paint sludge	15.00	40.27	43.41	1.32	11 855.51
Waste formaldehyde	7.50	0.40	91.04	1.06	15 571.23
Waste polyurethane	5.00	0.27	93.99	0.74	33 344.99
Refined chemical sludge	15.00	20.04	32.88	32.08	18 392.73
Antirust waste	10.00	4.57	81.04	4.39	27 346.59
Waste wood adhesive	15.00	10.75	53.44	20.82	16 963.28

Table 2 Average ultimate analysis of the wastes in Table 1

Moisture (%)	Ash (%)	C (%)	H (%)	N (%)	S (%)	O (%)	Cl (%)	LHV* (kJ/kg)
40.38	14.55	22.92	2.36	2.80	0.89	15.53	0.58	13050.27

* LHV: low heat value

3 Flame radiative property determination

The infrared camera, which was sensitive to radiation from 750 to 1350 cm^{-1}, was installed at the wall of the secondary combustion chamber, as shown in Fig. 2. In its spectral sensitivity range, the thermal radiation emitted from gases and particles is directional, so the effective emissivity $\bar{\varepsilon}$ of the flame is obtained by averaging the emissivities from different directions as

$$\bar{\varepsilon}=\frac{1}{\Delta\Omega}\int\varepsilon_{\hat{s}}\mathrm{d}\Omega\approx\frac{1}{\Delta\Omega}\sum_{i=1}^{N}\varepsilon_{\hat{s}_i}\mathrm{d}\Omega, \tag{1}$$

where $\Delta\Omega$ is the viewing angle of the camera and $\varepsilon_{\hat{s}_i}$ is the effective flame emissivity along the direction $\hat{\boldsymbol{s}}_i$ within a small solid angle $\mathrm{d}\Omega$, and N is the number of discrete directions in $\Delta\Omega$.

As the emissions from gases and particles are spectrally dependent, the effective emissivity in direction $\hat{\boldsymbol{s}}_i$ is formulated as (Modest, 2003)

$$\varepsilon_{\hat{s}}(S)=\int_0^\infty\varepsilon_{\hat{s},\eta}(S)\mathrm{d}\eta, \tag{2}$$

$$\begin{aligned}\varepsilon_{\hat{s},\eta}(S)&=\varepsilon_{\mathrm{w}}\exp\left(-\int_0^S\kappa_\eta\mathrm{d}\hat{\boldsymbol{s}}'\right)+1-\exp\left(-\int_0^S\kappa_\eta\mathrm{d}\hat{\boldsymbol{s}}'\right)\\&=\varepsilon_{\mathrm{w}}\exp\left[-\int_0^S(\kappa_{\eta,\mathrm{g}}+\kappa_{\eta,\mathrm{p}})\mathrm{d}\hat{\boldsymbol{s}}'\right]\\&\quad+1-\exp\left[-\int_0^S(\kappa_{\eta,\mathrm{g}}+\kappa_{\eta,\mathrm{p}})\mathrm{d}\hat{\boldsymbol{s}}'\right],\end{aligned} \tag{3}$$

where $\kappa_{\eta,\mathrm{g}}$ and $\kappa_{\eta,\mathrm{p}}$ are the monochromatic absorption coefficients of gases and particles, respectively, S is the geometric optical path length from the starting point at the refractory wall to the camera, and ε_{w} is the emissivity of the refractory wall.

In Eq. (3), it is implicitly assumed that the scattering of the particles is ignored and the radiative properties are calculated based on the path-average temperature, and the wall emission is diffusive. Similar assumptions have also been made by Grosshandler (1980) and Modest (1991) in calculating radiative heat transfer in inhomogeneous and non-isothermal media. The comparison made by Grosshandler between the exact value of the emissivity and those computed using the path-average temperature showed that even in the most unfavorable cases, the difference between them did not exceed 19%, and in many cases, it was just a fraction of 1%. Another thing that needs to be noted is that for a non-isothermal medium, the effective emissivity calculated from Eq. (3) is not a general property of the medium, but is optical path-dependent.

As the concentrations of gases and particles in the flame along the gas flow direction are non-uniform, to simplify the calculation, we divided the kiln into five sub-zones and indexed them from zone 1 to zone 5. The attached part of the secondary combustion chamber was indexed as zone 6. The gas and particle concentrations in each zone were considered to be uniform. The viewing angle of the camera was also separated into five small angles, from $\hat{\boldsymbol{s}}_0$ to $\hat{\boldsymbol{s}}_4$, with equal intervals, as illustrated in Fig. 2.

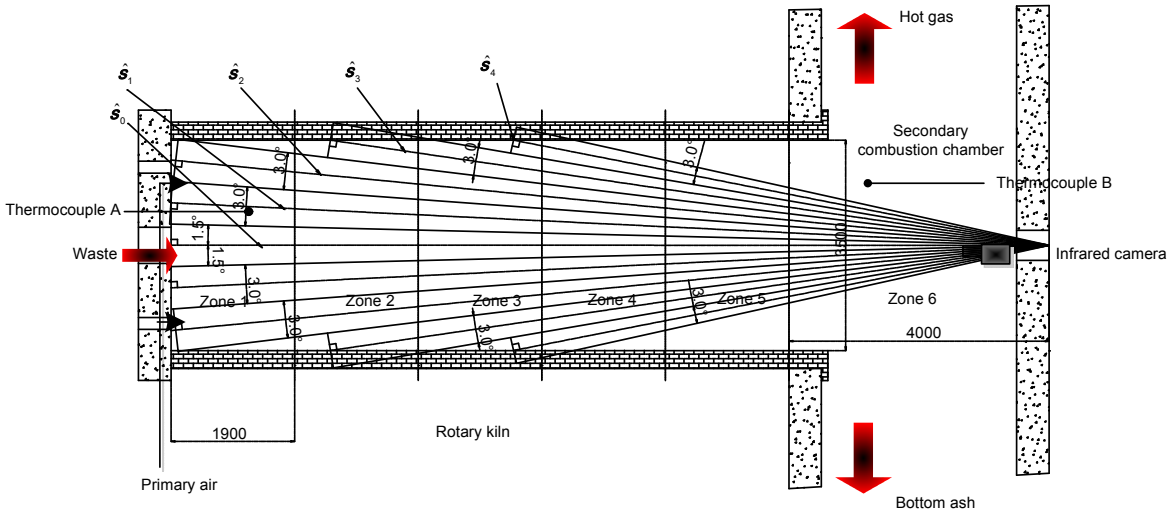

Fig. 2 Discrete combustion zone and discrete viewing angle of infrared camera (unit: mm)

Although the flame contains many different gas species, in the infrared range, most thermal radiation comes from CO_2 and H_2O because of their numerous absorption bands and large volume fractions. In this study, the combined narrow- and wide-band model proposed by Li and Tong (1995) was used to calculate the spectral absorption coefficient for a mixture of CO_2 and H_2O as

$$\kappa_{\eta,\mathrm{g}}=\frac{\rho(S_\mathrm{c}/\delta)\sinh(\pi\beta/2)}{\cosh(\pi\beta/2)-\cos[2\pi(\eta-\eta_\mathrm{c})/\delta]}, \tag{4}$$

where ρ is the gas volume density, η_c is the central wavenumber of the gas absorption band, and S_c/δ is the average absorption line intensity over the line spacing δ:

$$S_\mathrm{c}/\delta=(C_1/C_3)\exp(-a|\eta-\eta_\mathrm{c}|/C_3), \tag{5}$$

where a indicates the band type: a=1 for asymmetric bands and a=2 for symmetric bands. C_1 is the integrated band intensity and C_3 is the band width. β in Eq. (4) is the broadening parameter, and can be formulated as

$$\beta=C_2^2P_\mathrm{e}/(4C_1C_3), \tag{6}$$

and

$$P_\mathrm{e}=[p_\mathrm{T}/p_0+(b-1)p_\mathrm{a}/p_0]^n, \tag{7}$$

where p_a is the partial pressure of the gas, p_0 and p_T are the reference and total pressures, respectively, of the mixture, and C_2, b, and n are correlation parameters. More detailed descriptions of these parameters can be found in (Li *et al.*, 1995).

For the fly-ash particles contained in the flame, the absorption coefficient can be formulated as

$$\kappa_{\eta,\mathrm{p}}=\pi\int_0^\infty Q_\mathrm{abs}(\eta,r)r^2n(r)\mathrm{d}r, \tag{8}$$

where $n(r)$ is the particle number density distribution function. In this study, the modified γ-distribution, $n(r)=A\cdot r^\gamma\exp(-B\cdot r^\delta)$, was used. $Q_\mathrm{abs}(\eta, r)$ is the absorption cross-section of a single particle, which is calculated using the Mie method (Bohren and Huffman, 1983).

The detailed calculation of the effective flame emissivity in a rotary kiln burning solid waste can be summarized as follows.

Step 1: Set the air/waste equivalence ratio ϕ and determine the waste burnout rate for each zone.

Step 2: Calculate the gas species partial pressure in each zone:

$$p_{k,i}=\frac{V_{k,i}}{V_{\mathrm{gas},i}}\cdot p_0,\ k:\mathrm{CO_2},\mathrm{H_2O}, \tag{9}$$

where $V_{k,i}$ is the volume of gas k in zone i generated per kilogram of waste:

$$V_{k,i}=\alpha_i\cdot V_\mathrm{gas}^0\cdot\beta_{k,\mathrm{gas}}^0+(\phi-\alpha_i)\cdot V_\mathrm{air}^0\cdot\beta_{k,\mathrm{air}}^0, \tag{10}$$

where α_i is the local air/waste ratio for zone i, $\beta_{k,\mathrm{gas}}^0$ and $\beta_{k,\mathrm{air}}^0$ are the volumetric partial ratios of gas species k in the flame and supplied air under stoichiometric conditions, and $V_{\mathrm{gas},i}$ is the total gas volume:

$$V_{\mathrm{gas},i}=\alpha_i\cdot V_\mathrm{gas}^0+(\phi-\alpha_i)\cdot V_\mathrm{air}^0, \tag{11}$$

where V_gas^0 and V_air^0 are the theoretical volumes of flue gas and supplied air, respectively. These can be obtained from the ultimate analysis data for the waste mixture in Table 2 using the following equations:

$$\begin{aligned}V_\mathrm{air}^0=&0.0889\cdot(m_\mathrm{C}+0.375\cdot m_\mathrm{S})\\&+0.265\cdot m_\mathrm{H}-0.0333\cdot m_\mathrm{O},\end{aligned} \tag{12}$$

$$\begin{aligned}V_\mathrm{gas}^0=&0.01866\cdot(m_\mathrm{C}+0.375\cdot m_\mathrm{S})+0.79\cdot V_\mathrm{air}^0\\&+0.8\cdot m_\mathrm{N}/100+0.111\cdot m_\mathrm{H}\\&+0.0124\cdot m_\mathrm{moisture}+0.0161\cdot V_\mathrm{air}^0,\end{aligned} \tag{13}$$

where m_C, m_H, m_O, m_N and m_S are the ultimate weight compositions of carbon, hydrogen, oxygen, nitrogen and sulfur, respectively, and m_moisture is the water content.

Step 3: Determine the volume number density of the fly-ash particles in each zone. The number density function can be expressed as

$$n_i(r)=\frac{3}{4}\frac{f_\mathrm{v}(r)\cdot F_{\mathrm{p},i}}{\pi\cdot r^3}, \tag{14}$$

$$F_{\mathrm{p},i}=\frac{\alpha_i\cdot\chi\cdot m_{\mathrm{ash}}}{\rho_{\mathrm{ash}}\cdot V_{\mathrm{gas},i}}, \tag{15}$$

where $f_{\mathrm{v}}(r)$ is the volume fraction distribution function with respect to the particle radius, and $F_{\mathrm{v},i}$ is the volume fraction in zone i, which is calculated from the mass ratio χ of fly-ash particles in the total ash content.

Step 4: Calculate the monochromatic absorption coefficients of gases and fly-ash particles according to the band model and Mie method, based on the path-average temperature:

$$\exp\left(-\int_0^{S_i}k_{\eta,\mathrm{g}}\mathrm{d}\hat{s}'\right)=\exp\left(-\sum_{j=1}^{6}(\kappa_{\eta,\mathrm{g},j})\cdot\Delta L_{j,i}\right), \tag{16a}$$

$$\exp\left(-\int_0^{S_i}k_{\eta,\mathrm{p}}\mathrm{d}\hat{s}'\right)=\exp\left(-\sum_{j=1}^{6}(\kappa_{\eta,\mathrm{p},j})\cdot\Delta L_{j,i}\right), \tag{16b}$$

where $\kappa_{\eta,\mathrm{g},j}$ and $\kappa_{\eta,\mathrm{p},j}$ are the monochromatic absorption coefficients of the gas and particles in zone j, respectively, and $\Delta L_{j,i}$ is the geometric length of path $\hat{\boldsymbol{s}}_i$ in zone j.

Step 5: Calculate the flame emissivities along different optical paths through spectral integration, and calculate the band effective emissivity of the flame in the kiln, based on Eq. (1):

$$\varepsilon_{\hat{\boldsymbol{s}}}(S_i)=\int_{\eta_1}^{\eta_2}\varepsilon_{\hat{\boldsymbol{s}},\eta}(S_i)\mathrm{d}\eta, \tag{17}$$

$$\overline{\varepsilon}=\frac{1}{\Delta\Omega}\sum_{i=0}^{4}\varepsilon_{\hat{s}_i}\mathrm{d}\Omega_j, \tag{18}$$

where η_1 and η_2 are the lower and upper values of the spectral sensitivity range of the camera, respectively. Then $\overline{\varepsilon}$ can be used for thermographic temperature measurements.

4 Results and discussion

As mentioned in the previous section, the chamber of the rotary kiln and the viewing angle of the camera were divided into six sub-zones and five sub-angles, respectively, as shown in Fig. 2. According to the above calculation steps, in order to determine the gas and particle compositions in the flame for radiative property calculations, the air/waste equivalence ratio and burnout rate of the waste in each zone should be known first. In this study, three air/waste equivalence ratios, 1.0, 1.4, and 1.8, were set by adjusting the supplied air. The waste burnout rates of zone 1 and zone 6 were measured by direct sampling analysis. The results were approximately 0.5 and 1.0, respectively. The burnout rates of other zones were then deduced by linear interpolation. The mass ratio of fly-ash particles measured by the gas sampling method was approximately 20% of the total ash content. After the air/waste ratio and burnout rate were known, we calculated the flame temperature and path-average temperature and flame compositions based on the waste components in Table 2, according to the heat and mass balance theory (Law, 2006). The total gas pressure in the incinerator was kept at about 100 Pa below ambient atmospheric pressure to avoid leakage of hot gas. The wall temperatures of different zones were set to be the same as the flame temperature in the same zone, and the wall emissivity was about 0.76, depending on the material (Modest, 2003).

The pressures of CO_2 and H_2O, and the volume fraction of fly-ash particles in different zones for three air/waste equivalence ratios are plotted in Fig. 3. All the values increased linearly from zone 1 to zone 6 as the burnout rate increased from 0.5 to 1.0. When the air/waste equivalence ratio increased from 1.0 to 1.8, the gas pressure and particle volume fraction decreased quickly because the flame gas was diluted by abundant excess air. The volume fraction of the fly-ash particle cloud in the flame was approximately 7.5×10^{-6} under chemical equilibrium combustion conditions.

The spectral radiative properties of the particles and gases under stoichiometric conditions (ϕ=1.0) are given in Fig. 4. For the particles, the complex refractive index required by the Mie method was determined using Chang (1995)'s equation.

Figs. 4a and 4b show the spectral radiative coefficients and scattering phase functions of the fly-ash cloud for different wavenumbers. Because of the relatively small volume fraction, the absorption and scattering coefficients of the fly-ash cloud are relatively small, and the scattering is approximately twice as strong as the absorption. From the scattering phase function of the fly-ash cloud at five typical wavenumbers, we can see that more than 90% of the total

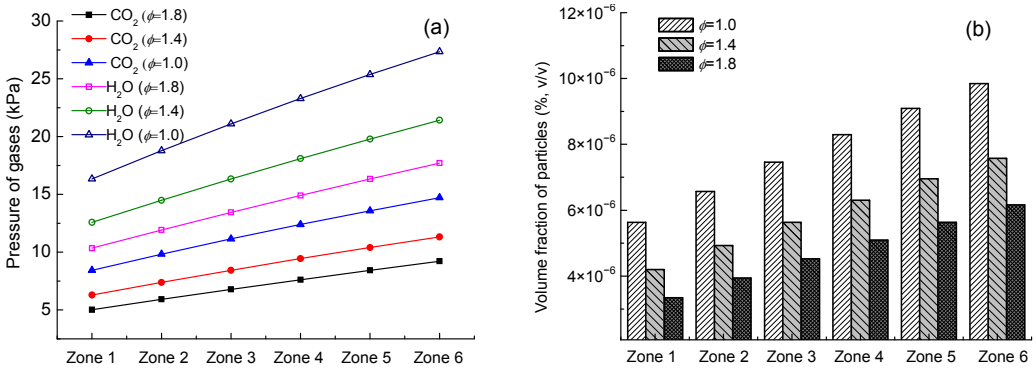

Fig. 3 Initial data for different zones
(a) Partial pressures of gases; (b) Volume fractions of particles

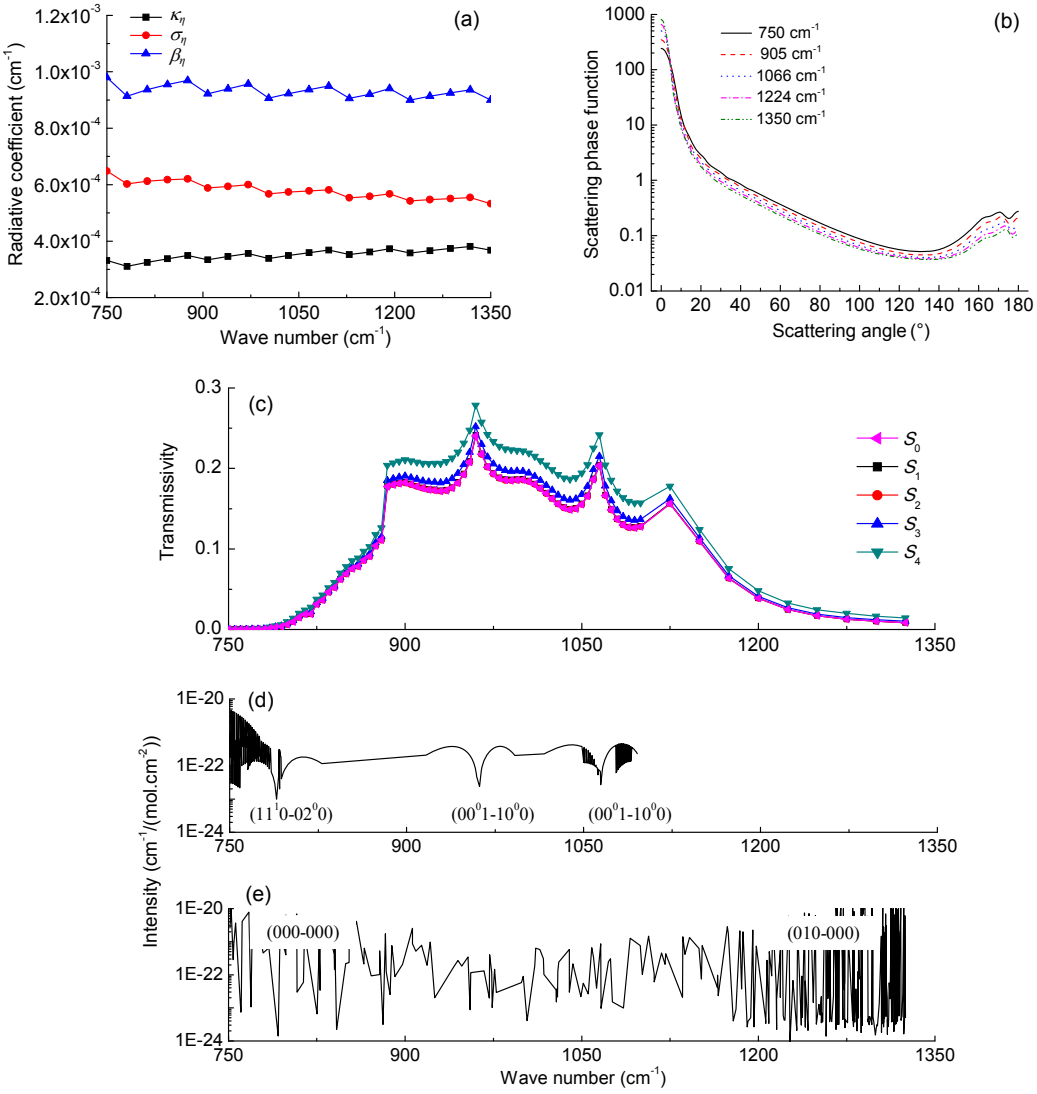

Fig. 4 Radiative properties of flame for ϕ=1.0
Radiative coefficients (a) and scattering phase functions (b) of fly-ash particles; Spectral transmissivities of gases along different directions (c); Absorption line intensities of CO_2 (d) and H_2O (e)

scattered energy was redirected forward within a cone of 10° from the direction of transmission. Modest (2003) suggested that in heat transfer applications, we may neglect such scattering effects and treat them as transmission. Thus, neglecting the fly-ash scattering in Eq. (3) is reasonable.

For gases, the spectral transmissivity under different directions is illustrated, along with the absorption line intensity selected from the HITEMP database (Figs. 4c–4e) (Rothman *et al.*, 2010). The absorption of the gases between 750 and 1350 cm^{-1} was dominated by the ($11^{1}0$-$02^{0}0$), ($00^{0}1$-$10^{0}0$), and ($00^{0}1$-$10^{0}0$) bands of CO_2, and (000-000) and (010-000) bands of H_2O. The spectral transmissivities in different directions were very similar and inversely proportional to the geometric path length. A discrepancy appears between 850 and 1100 cm^{-1}, where the absorption was relatively weak.

When the wavenumber is less than 800 cm^{-1} or larger than 1200 cm^{-1}, the gas becomes non-transparent because the geometric path length is larger than the optical thickness as a result of the strong absorptions of CO_2 and H_2O.

The integrated spectral transmissivities of gases and particles over the viewing angle of the infrared camera are plotted in Fig. 5. Because the pressures of CO_2 and H_2O in the flame were diluted by infrared transparent N_2 and O_2 from excess air, the transmissivity of the flame increases with equivalence ratio, especially between 850 and 1100 cm^{-1}. The peak of the spectrum appears near 950 cm^{-1}. Fig. 5 also gives the transmissivity without particles. Compared with gases, the absorption caused by the fly-ash cloud is ignorable. The maximum relative difference at 975 cm^{-1} is less than 1.5%. Such a negligible difference is expected because of the small volume fraction of fly-ash particles in the flame.

Based on the spectral transmissivity, the effective flame emissivities under different air/waste equivalence ratios were deduced and results are shown in Fig. 6. For the waste components discussed in this study, the effective emissivity changed from 0.89 to 0.80 when the air/waste equivalence ratio increased from 1.0 to 1.8, which is very close to the emissivities used by other researchers for similar flames (Manca and Rovaglio, 2002; Planas-Cuchi *et al.*, 2003). However, as thermographic temperature measurements are very sensitive to flame emissivity, we suggested a fitting function to relate the flame emissivity to the air/waste equivalence ratio:

$$\bar{\varepsilon} = 1.0944 - 0.25225 \times \phi + 0.04957 \times \phi^2, \quad \phi \in [1.0, 1.8]. \tag{19}$$

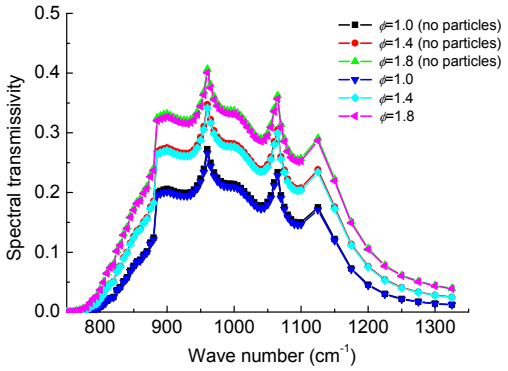

Fig. 5 Spectral transmissivities with and without particles under different air/waste equivalence ratios

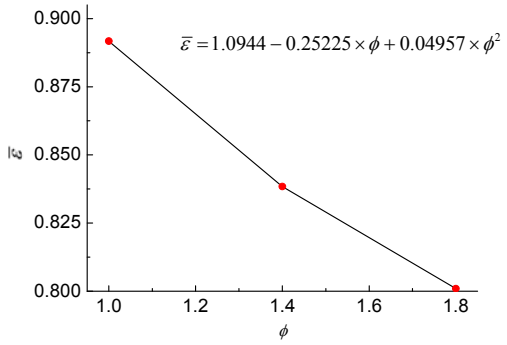

Fig. 6 Fitting curve of effective flame emissivity with respect to air/waste equivalence ratio

This equation was used for adjusting the flame emissivity to improve the on-line flame temperature measurement accuracy, because when the heat value of the waste is maintained at a constant level, the effective flame emissivity only depends on the air/waste ratio. Fig. 7 shows thermographic temperature images with different emissivity settings of the flame in the kiln burning the same waste discussed in this study, for ϕ=1.28. According to Eq. (19), the correct flame emissivity should be 0.85, and the temperature would be overestimated with an emissivity smaller than 0.85 and underestimated with an emissivity larger than 0.85. The maximum measurement discrepancy with an incorrect emissivity would exceed 100 °C.

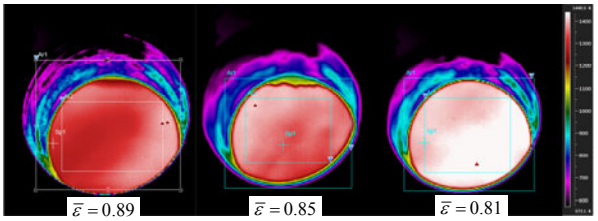

Fig. 7 Flame thermographic images with different emissivity settings

To evaluate the temperature measurement accuracy, fifty thermographic images were captured and post-processed with different flame emissivities calculated using Eq. (19). The average temperature was compared with that measured by thermocouple B installed at the rear part of the kiln (Figs. 1 and 2). The temperatures obtained using these two methods under different air/waste equivalence ratios are plotted in Fig. 8. If the flame emissivity is set to be constant, the temperature would be underestimated for the flame with an increased air/waste equivalence ratio, and over-measured with a decreased ratio. The maximum variance of the flame temperature would exceed 90 °C, which could cause operational problems such as slagging and refractory failure. If the emissivity is adjusted according to Eq. (19), the temperature measurement accuracy is significantly improved.

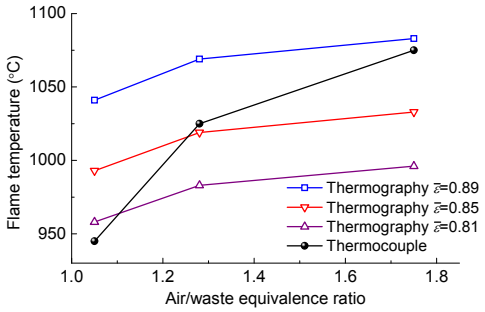

Fig. 8 Flame temperatures measured using thermocouple and thermographic cameras with different flame emissivity settings

5 Conclusions

Accurate and fast flame temperature measurement is essential for the safety of waste-incineration systems and pollutant control. A non-intrusive thermographic method using an infrared camera is the most promising method for achieving accurate real-time temperature measurements. However, the measurement accuracy of the thermographic method strongly depends on the flame emissivity setting. In this study, the effective flame emissivity in a rotary kiln incinerator burning hazardous solid waste under different air/waste equivalence ratios was investigated numerically, using a combined narrow- and wide-band model and Mie method. The results show that the spectral transmissivity of the heterogeneous combustion flame in the kiln is dominated by H_2O and CO_2 in the infrared range. The effects of fly-ash particles on the effective emissivity are ignorable. A fitting function for flame emissivity with respect to the air/waste equivalence ratio was proposed. Experimental measurement results suggested that the temperature measurement accuracy could be greatly improved by adjusting the flame emissivity setting according to the air/waste equivalence ratio.

References

Águeda, A., Pastor, E., Pérez, Y., Planas, E., 2010. Experimental study of the emissivity of flames resulting from the combustion of forest fuels. *International Journal of Thermal Sciences*, **49**(3):543-554. [doi:10.1016/j.ijthermalsci.2009.09.006]

Ballester, J., Garcia-Armingol, T., 2010. Diagnostic techniques for the monitoring and control of practical flames. *Progress in Energy and Combustion Science*, **36**(4):375-411. [doi:10.1016/j.pecs.2009.11.005]

Bohren, C.F., Huffman, D.R., 1983. Absorption and Scattering of Light by Small Particles. John Wiley & Sons, New York, p.128.

Buekens, A., Huang, H., 1998. Comparative evaluation of techniques for controlling the formation and emission of chlorinated dioxins/furans in municipal waste incineration. *Journal of Hazardous Materials*, **62**(1):1-33. [doi:10.1016/S0304-3894(98)00153-8]

Chang, F.C., Rhodes, C.A., 1995. Computer Modeling of Radiation and Combustion in a Rotary Solid-Waste Incinerator. Argonne National Lab, US Department of Energy Report ANL/ET/CP-85778.

Docquier, N., Candel, S., 2002. Combustion control and sensors: a review. *Progress in Energy and Combustion Science*, **28**(2):107-150. [doi:10.1016/S0360-1285(01)00009-0]

Edwards, D.K., 1962. Radiation interchanges in a non-gray enclosure containing an isothermal carbon dioxide and nitrogen gas mixture. *Journal of Heat Transfer*, **84**(1):1-11. [doi:10.1115/1.3684283]

Edwards, D.K., Balakrishnan, A., 1973. Thermal radiation by combustion gases. *International Journal of Heat and Mass Transfer*, **16**(1):25-40. [doi:10.1016/0017-9310(73)90248-2]

GB 18484-2001, 2005. Pollution Control Standard for Hazardous Waste Incineration. Ministry of Environmental Protection and General Administration of Quality Supervision, Inspection and Quarantine of the People's Republic of China. China Environmental Press, Beijing.

Gohlke, O., Busch, M., 2001. Reduction of combustion by-products in WTE plants: O_2 enrichment of under fire air in the Martin Syncom process. *Chemosphere*, **42**: 545-550. [doi:10.1016/S0045-6535(00)00226-5]

Grosshandler, W.L., 1980. Radiative heat transfer in inhomogeneous gases: A simplified approach. *International Journal of Heat and Mass Transfer*, **23**(11):1447-1459. [doi:10.1016/0017-9310(80)90149-0]

HJ/T176-2005. Technical Specifications for Centralized Incineration Facility Construction on Hazardous Waste. Ministry of Environmental Protection of the People's Republic of China. China Environmental Press, Beijing.

Law, C.K., 2006. Combustion Physics. Cambridge University Press, New York, p.31-49.

Li, W., Tong, T.W., 1995. A combined narrow- and wide-band model for computing the spectral absorption coefficient of CO_2, CO, H_2O, CH_4, C_2H_2, and NO. *Journal of Quantitative Spectroscopy and Radiative Transfer*, **54**(6): 961-970. [doi:10.1016/0022-4073(95)00126-6]

Manca, D., Rovaglio, M., 2002. Infrared thermographic image processing for the operation and control of heterogeneous combustion chambers. *Combustion and Flame*, **130**: 277-297. [doi:10.1016/S0010-2180(02)00372-3]

Modest, M.F., 1991. The weighted-sum-of-gray-gases model for arbitrary solution methods in radiative transfer. *Journal of Heat Transfer*, **113**(3):650-656. [doi:10.1115/1.2910614]

Modest, M.F., 2003a. Radiative Heat Transfer. McGraw Hill, New York, p.288-357.

Modest, M.F., 2003b. Radiative Heat Transfer (2nd Ed.). Academic, New York, p.287-410.

China Statistical Yearbook on Environment, 2009. National Bureau of Statistics and Ministry of Environmental Protection of the People's Republic of China. China Statistics Press, Beijing.

Ni, Y.W., Zhang, H.J., Fan, S., Zhang, X.P., Zhang, Q., Chen, J.P., 2009. Emissions of PCDD/Fs from solid waste incinerators in China. *Chemosphere*, **75**(9):1153-1158. [doi:10.1016/j.chemosphere.2009.02.051]

Parent, G., Acem, Z., Lechêne, S., Boulet, P., 2010. Measurement of infrared radiation emitted by the flame of a vegetation fire. *International Journal of Thermal Sciences*, **49**(3):555-562. [doi:10.1016/j.ijthermalsci.2009.08.006]

Planas-Cuchi, E., Chatris, J.M., López, C., Arnaldos, J., 2003. Determination of flame emissivity in hydrocarbon pool fires using infrared thermography. *Fire Technology*, **39**(3):261-273. [doi:10.1023/A:1024193515227]

Rothman, L.S., Gordon, I.E., Barber, R.J., Dothe, H., Gamache, R.R., Goldman, A., Perevalov, V., Tashkun, S.A., Tennyson, J., 2010. HITEMP, the high-temperature molecular spectroscopic database. *Journal of Quantitative Spectroscopy and Radiative Transfer*, **111**(15):2139-2150. [doi:10.1016/j.jqsrt.2010.05.001]

Subramanya, M., Choudhuri, A.R., 2004. Operating Point Control of Combustion Processes Using Dynamic Flame Tracking. 2nd International Energy Conversion Engineering Conference, AIAA, p.5523.

Sudheer, S., Prabhu, S.V., 2010. Measurement of flame emissivity of gasoline pool fires. *Nuclear Engineering and Design*, **240**(10):3474-3480. [doi:10.1016/j.nucengdes.2010.04.043]

Vosteen, B., Beyer, J., Bonkhofer, T., 2002. Simultaneous inner and outer thermography of rotary kilns for hazardous waste incineration. *VGB PowerTech*, **9**:71-77.